IEEE Access
Multidisciplinary ⋮ Rapid Review ⋮ Open Access Journal

Received 15 August 2023, accepted 14 September 2023, date of publication 19 September 2023,
date of current version 28 September 2023.

Digital Object Identifier 10.1109/ACCESS.2023.3317086

RESEARCH ARTICLE

Dynamic Characteristics and Stability of the Photovoltaic Cell Under Laser Intensity or Load Disturbance in Laser Wireless Power Transmission System

ZHENYANG XIONG[1,2], RONG CAI[1,2], XING DU[1,2], HAO DU[1], AND GUONING XU[1,2], (Senior Member, IEEE)

[1]Aerospace Information Research Institute, Chinese Academy of Sciences, Beijing 100094, China
[2]University of Chinese Academy of Sciences, Beijing 100049, China

Corresponding author: Guoning Xu (xugn@aircas.ac.cn)

This work was supported by the Strategic Priority Research Program of the Chinese Academy of Science under Grant XDA17020304.

ABSTRACT In laser wireless power transmission (LWPT) system, the dynamically varying laser intensity or load on the photovoltaic (PV) cell may result in significant decrease of the power, efficiency and stability. The explicit steady and dynamic *I*-*V* characteristic equations are proposed innovatively to study the dynamic output characteristics and the stability of the PV cell under laser intensity or equivalent load disturbance. The time-domain response equations of photocurrent and dark current under large signal step disturbance are deduced. And the frequency-domain small signal model of the PV cell is derived to calculated the output impedance. The results suggest that the dynamic response time and the steady-state current of the photocurrent increase with the carrier lifetime. The PV cell under the high-frequency disturbance may result in the instability of the LWPT system. The models and methods will provide basis for the simulation and optimization of the DC-DC converter and the closed loop controller to improve the dynamic characteristics and stability of the LWPT system.

INDEX TERMS Laser wireless power transmission, photovoltaic cell, equivalent circuit model, dynamic characteristic, stability, equivalent output impedance.

I. INTRODUCTION

Laser has the advantage of high-power density, remarkable collimation, and energy concentration, which make it an effective tool for transmitting energy over long distances in both space and the atmosphere [1]. The laser wireless power transmission (LWPT) technology has a wide range of potential scenarios for energy supply for aerostats and unmanned aerial vehicles, arousing an increasing research interest [2], [3].

The schematic diagram depicting the components of the LWPT system is presented in FIGURE 1. The PV cell serves as the pivotal device for photovoltaic conversion within the LWPT system. Its efficiency and output characteristics are significantly influenced by the laser intensity and self-performance. In addition, the PV array acts as an input source for the DC-DC converter. It is crucial to understand the output current and voltage (*I*-*V*) characteristics of the PV cell for the design of the DC-DC converter, maximum power point tracking (MPPT) algorithm, and closed-loop control circuit within the LWPT system [4].

The atmospheric turbulence and aerosols can cause significant fluctuations in laser intensity and distortions in the laser spot during laser transmission through the atmosphere. [5], [6]. And the PV cell receives intermittent laser when the laser beam disengages and recaptures the PV array. These factors lead to the dynamic fluctuations of laser intensity received by the PV cell. In addition, the principle of the MPPT

The associate editor coordinating the review of this manuscript and approving it for publication was Shuo Sun.

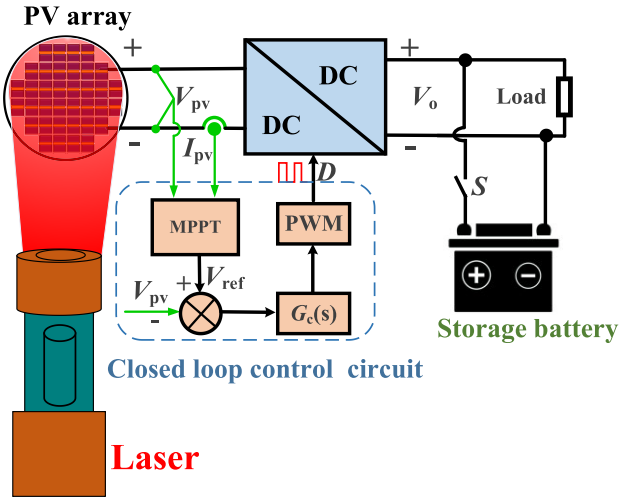

FIGURE 1. The schematic diagram depicting the components of the LWPT system.

is to change the equivalent load at the output interface of the PV array by controlling the duty cycle D of the DC-DC converter. The dynamically varying laser intensity or load will cause the instability of the output voltage and current of the PV cell, which includes the switch of the operating point on different I-V curves or high frequency fluctuation near the specific static operating point. These disturbances will cause the voltage and current at maximum power point (MPP) cannot be accurately sampled and obtained, which may lead to ineffectiveness of the MPPT algorithm and the oscillation of the system. And the closed-loop control circuit may be invalid to maintain the stability of system. As a consequence, the electric energy generated by the PV cell cannot be utilized efficiently and will be lost in the form of heat energy. Meanwhile, the voltage and current stress of the power components in the DC-DC converter will increase dramatically. According to FIGURE 1, the LWPT system is compose by the PV cell, the DC-DC converter and the back-end load in cascades. The mismatch between the output impedance of the PV cell and the input impedance of the DC-DC converter will also destroy the stability of the system. Therefore, it is essential to study the dynamic output characteristics and stability of the PV cell under disturbances to obtain the output impedance and the dynamic response time of the output voltage and current, which will provide the basis design the MPPT algorithm, DC-DC converter and the closed-loop control circuit.

Many scholars have studied the variation on performance of the PV cell such as open-circuit voltage, short-circuit current, maximum power point voltage, current and photoelectric conversion efficiency with solar irradiance and temperature through modeling and experiments [7], [8], [9], [10]. These methods can accurately calculate the static output characteristics of the PV cell, but the dynamic performance cannot be accurately obtained. On the basis of the photoelectric conversion principle of the PV cell, researchers established the equivalent circuit models to study its output characteristics. In particular, single-diode model [11], double-diode model [12] and triple-diode model [13] brought about widespread attention. However, the voltage and current equations in these equivalent models are transcendental equations, and the exact expression of the output voltage and current cannot be obtained directly by analytical method. Therefore, to study the output characteristics of PV cell, the approximate methods are usually used in practical application by omitting the terms with minuscule values in the transcendental equation. And then the implicit equation is made explicit to reduce calculation complexity, but the representation accuracy will decrease [14], [15], [16]. Lambert W function can be used to make the implicit transcendental equation explicit, and then the explicit expressions of voltage and current can be obtained, but the computational process is complicated [17], [18]. Therefore, it is essential to design a simple and accurate method to obtain the output characteristics of the PV cell. Moreover, some scholars have measured the dynamic characteristics and stability process of PV cell through experiments. That is, to give a small disturbance on the forward bias voltage of the PV cell and to synchronously detect the current. Or the output voltage of the PV cell is detected synchronously by changing the incident light intensity [19], [20]. Qin analyzed the dynamic characteristics and stability of the solar cell by modeling, derived the equivalent circuit model of the solar cell based on the PN junction physical principles, and gave the expression of the model parameters [21]. Due to ignoring the photogenerated carrier in N-region, there will be a significant error to represent the output characteristics of the PV cell under high intensity laser. However, the transport states of the photogenerated carriers are more complex, and the generation and recombination of which are more significant in the PV cell under the unstable high energy density laser beam irradiation. The parasitic resistance, capacitance and inductance of the PV cell have an undesirable influence on its dynamic output characteristics [22], [23]. At present, there are few studies on the output characteristics and stability of the PV cell under laser intensity or load disturbance.

To address these issues, this paper creatively deduced the explicit output characteristics equations of the PV cell under static state, dynamic small-signal and large-signal disturbance. The equivalent circuit models are proposed. And then, the model parameters are identified and the output characteristics of the PV cell are investigated. Furthermore, based on the small signal model, its equivalent output impedance is derived, the stability of the PV cell and the LWPT system are studied. Finally, the large signal model of the PV cell is established, and the nonlinear I-V curve is linearized, which will simplify the modeling and analysis of the dynamic characteristic of the LWPT system.

The remainder of this paper is structured as follows: Section II presents the theory and method mainly including the mathematical model and equivalent circuit model of

TABLE 1. Nomenclature and values.

Symbol	Quantity	Value
D_n	Electron diffusion coefficients	220 cm^2/s
D_p	Hole diffusion coefficients	10.4 cm^2/s
n_i	Intrinsic carrier density	1.8×10^6 cm^{-3}
α	Absorption coefficient	1.4×10^4 cm^{-1}
τ_{n0}	Minority electron lifetime in the p region	10^{-9}~10^{-8} s
τ_{p0}	Minority hole lifetime in the n region	10^{-9}~10^{-8} s
μ_n	Electron drift mobility	8500 $cm^2/V\cdot s$
μ_p	Hole drift mobility	400 $cm^2/V\cdot s$
L_n	Electron diffusion length	$\sqrt{D_n\tau_n}$ m
L_p	Hole diffusion length	$\sqrt{D_p\tau_p}$ m
x_n	Depletion width in the n region	2×10^{-9} m
x_p	Depletion width in the p region	8×10^{-9} m
W_n	Thickness of the n region	50×10^{-9} m
W_p	Thickness of the p region	200×10^{-9} m
A	Area of the PV cell	12 cm^2
N_D	Doping concentration in N region	1×10^{18} cm^{-3}
N_A	Doping concentration in P region	5×10^{17} cm^{-3}
q	Electron charge	1.602×10^{-19} C
λ	The wavelength of the laser	808×10^{-9} m
c	Photon speed	3×10^8 m/s
h	Planck constant	6.63×10^{-34} J·s
k	Boltzmann constant	1.381×10^{-23} J/K
T	Cell temperature	300 K
Φ_0	Photon flux density on the PV cell	$cm^{-2}\cdot s^{-1}$
P	Incident Laser power	W
η_0	Photon absorption rate of the PV cell	90%
R_s	Series resistance	Ω
R_{sh}	Shunt resistance	Ω
L	Parasitic inductance	1 uH
I_{d1}, I_{d2}	Diode current	A
I_{o1}, I_{o2}	Reverse saturation current	A
V_{oc}	Open circuit voltage of the PV cell	V
I_{sc}	Short circuit current of the PV cell	A
I_{ph}	Photocurrent of the PV cell	A
I_{mpp}	Maximum power point current	A
V_{mpp}	Maximum power point voltage	V
I	Output current of the PV cell	A
V	Output voltage of the PV cell	A
V_d	Diode positive guide pass voltage drop	V

the PV cell and the LWPT system under different working conditions. Section III analyses and examines the numerical results. Finally, Section IV summarizes the conclusions drawn from the study.

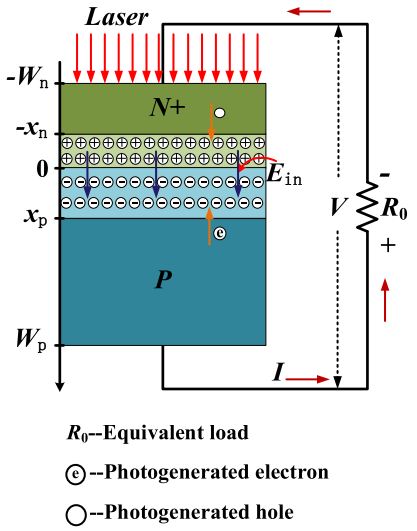

FIGURE 2. Photoelectric conversion principle of the PV cell.

II. THEORY AND METHOD

A. STATIC MATHEMATICAL MODEL AND EQUIVALENT CIRCUIT OF THE PV CELL

The material of the PV cell is gallium arsenide (GaAs). The parameters of the PV cell and the laser are shown in Table 1. The physical structure and photoelectric conversion principle of the PV cell are shown in FIGURE 2. Under the laser irradiance, the N region, P region and space charge region of the PV cell absorb the photon, excite electrons of the semiconductor atom from the valence band to the conduction band, and continuously produce photo-generated excess carriers.

Under the action of concentration gradient, the photo-generated excess holes in N-region and the photo-generated excess electrons in P-region diffuse to the space charge region and form the diffusion current. Further, the photo-generated excess holes drift to the P region, and the excess minority electrons drift to the N region under the internal electric field E_{in} of the space charge region. Then, the electric potential in the N region decreases and in the P region increases, which forms the photon-induced voltage.

Continuous photogenerated current is generated in the loop under the action of photogenerated electromotive force when the PV cell connected with external load forming a closed loop. During the continuous movement of the excess carrier electrons and holes in the space charge region, they will inevitably collide and recombine to generate recombination current I_{rec}. According to the photoelectric conversion process of the PV cell, the output current I is the photogenerated current I_{ph} minus the recombination current I_{rec}. The output current I flows through the load R_0 to generate the voltage V, which makes the PN junction positively biased. That is, the forward bias voltage of the PV cell.

The diffusion current is determined by the concentration gradient of the excess carrier. For the particular material,

the concentration of photo-generated excess carriers depends on the incident laser photon flux density, temperature, and external electric field strength in the PV cell. When these parameters change with time t, the excess carrier concentration is a function of time and space [24]. Which satisfies equation (1) and (2).

$$\frac{\partial \delta n(x,t)}{\partial t} = D_{\mathrm{n}}\frac{\partial^2 \delta n(x,t)}{\partial x^2} + \mu_{\mathrm{n}}E(x,t)\frac{\partial \delta n(x,t)}{\partial x} + g_{\mathrm{n}}(x,t) - \frac{\delta n(x,t)}{\tau_{\mathrm{n}}} \tag{1}$$

$$\frac{\partial \delta p(x,t)}{\partial t} = D_{\mathrm{p}}\frac{\partial^2 \delta p(x,t)}{\partial x^2} + \mu_{\mathrm{p}}E(x,t)\frac{\partial \delta p(x,t)}{\partial x} + g_{\mathrm{p}}(x,t) - \frac{\delta p(x,t)}{\tau_{\mathrm{p}}} \tag{2}$$

where, $g_{\mathrm{n}}(x,t)$ and $g_{\mathrm{p}}(x,t)$ are the generation rate of minority carriers in the P region and in N region.

$$\begin{aligned} g_{\mathrm{n}}(x,t) &= \phi_0\eta_0 \mathrm{e}^{-\alpha(\mathrm{W_n}+x_{\mathrm{p}})}\alpha \mathrm{e}^{-\alpha(x-x_{\mathrm{p}})} \\ &= \eta_0\frac{P\lambda}{Ahc}\alpha \mathrm{e}^{-\alpha(x+\mathrm{W_n})}, (x_{\mathrm{p}} \le x \le W_p) \end{aligned} \tag{3}$$

$$\begin{aligned} g_{\mathrm{p}}(x,t) &= \phi_0\eta_0 \mathrm{e}^{-\alpha(\mathrm{W_n}-x_{\mathrm{n}})}\alpha \mathrm{e}^{-\alpha(x+x_{\mathrm{n}})} \\ &= \eta_0\frac{P\lambda}{Ahc}\alpha \mathrm{e}^{-\alpha(x+\mathrm{W_n})}, (-W_{\mathrm{n}} \le x \le -x_{\mathrm{n}}) \end{aligned} \tag{4}$$

where, $\delta n(x,t)$ and $\delta p(x,t)$ are the concentration of photo-generated excess minority carriers in P region and N region, respectively. Eq. (5) can be obtained when laser power P and temperature T are constant.

$$\begin{cases} \frac{\partial \delta n(x,t)}{\partial t} = 0 \\ \frac{\partial \delta p(x,t)}{\partial t} = 0 \end{cases} \tag{5}$$

Substituting Eqs (3)-(5) into Eqs (1) and (2). Eqs (6) and (7) can be obtained:

$$\begin{aligned} \delta n(x) &= n_{\mathrm{p0}}\left(\mathrm{e}^{\frac{qV}{kT}} - 1\right)\mathrm{e}^{\frac{x_{\mathrm{p}}-x}{L_{\mathrm{n}}}} \\ &+ \frac{-\eta_0 P\lambda\tau_{\mathrm{n}}\alpha \mathrm{e}^{-\alpha(W_{\mathrm{n}}+x_{\mathrm{p}})}}{Ahc\left(\alpha^2 L_{\mathrm{n}}^2 - 1\right)}\mathrm{e}^{-\alpha(x-x_{\mathrm{p}})} \end{aligned} \tag{6}$$

$$\begin{aligned} \delta p(x) &= p_{\mathrm{n0}}\left(\mathrm{e}^{\frac{qV}{kT}} - 1\right)\mathrm{e}^{\frac{x_{\mathrm{n}}+x}{L_{\mathrm{p}}}} \\ &+ \frac{-\eta_0 P\lambda\tau_{\mathrm{p}}\alpha \mathrm{e}^{-\alpha(W_{\mathrm{n}}-x_{\mathrm{n}})}}{Ahc\left(\alpha^2 L_{\mathrm{p}}^2 - 1\right)}\mathrm{e}^{-\alpha(x+x_{\mathrm{n}})} \end{aligned} \tag{7}$$

The output current of the PV cell is the sum of the photo-generated excess carrier hole current at $x = -x_{\mathrm{n}}$ and the photo-generated excess carrier electron current at $x = x_{\mathrm{p}}$, minus the recombination current of electron and hole in the space charge region [24], which can be expressed as

$$\begin{aligned} I &= A \times \left[J_{\mathrm{p}}(-x_{\mathrm{n}}) + J_{\mathrm{n}}(x_{\mathrm{p}}) - J_{\mathrm{rec}}\right] \\ &= -qAD_{\mathrm{p}}\frac{\mathrm{d}(\delta p(x))}{\mathrm{d}x}|_{x=-x_{\mathrm{n}}} + qAD_{\mathrm{n}}\frac{\mathrm{d}(\delta n(x))}{\mathrm{d}x}|_{x=x_{\mathrm{p}}} - AJ_{\mathrm{rec}} \end{aligned} \tag{8}$$

Based on the Shockley-Read-Hall (SRH) model [25], the recombination rate r of the excess electrons and holes at the center of the space charge region under forward biased voltage can be expressed as [24].

$$r = \frac{n_{\mathrm{i}}}{2\sqrt{\tau_{\mathrm{n0}}\tau_{\mathrm{p0}}}}\frac{\mathrm{e}^{\frac{qV}{kT}} - 1}{\mathrm{e}^{\frac{qV}{2kT}} - 1} \tag{9}$$

The recombination current density can be obtained from Eq. (10) [24]:

$$\begin{aligned} J_{\mathrm{rec}} &= \int_{-x_{\mathrm{n}}}^{x_{\mathrm{p}}} qr\mathrm{d}x = \frac{qn_{\mathrm{i}}\left(x_{\mathrm{p}}+x_{\mathrm{n}}\right)}{2\sqrt{\tau_{\mathrm{n0}}\tau_{\mathrm{p0}}}}\frac{\mathrm{e}^{\frac{qV}{kT}} - 1}{\mathrm{e}^{\frac{qV}{2kT}} + 1} \\ &= \frac{qn_{\mathrm{i}}\left(x_{\mathrm{p}}+x_{\mathrm{n}}\right)}{2\sqrt{\tau_{\mathrm{n0}}\tau_{\mathrm{p0}}}}\left(\mathrm{e}^{\frac{qV}{2kT}} - 1\right) \end{aligned} \tag{10}$$

Substituting Eq. (6), Eq. (7) and Eq. (10) into the Eq. (8), the explicit expression of the ideal model for the PV cell can be obtained:

$$\begin{aligned} I &= \frac{\eta_0 P\lambda q D_{\mathrm{p}}\alpha^2\tau_{\mathrm{p}}}{hc\left(\alpha^2 L_{\mathrm{p}}^2 - 1\right)}\mathrm{e}^{-\alpha(W_{\mathrm{n}}-x_{\mathrm{n}})} + \frac{\eta_0 P\lambda q D_{\mathrm{n}}\alpha^2\tau_{\mathrm{n}}}{hc\left(\alpha^2 L_{\mathrm{n}}^2 - 1\right)}\mathrm{e}^{-\alpha(W_{\mathrm{n}}+x_{\mathrm{p}})} \\ &- \left(\frac{qAD_{\mathrm{p}}p_{\mathrm{n0}}}{L_{\mathrm{p}}} + \frac{qAD_{\mathrm{p}}n_{\mathrm{p0}}}{L_{\mathrm{n}}}\right)\left(\mathrm{e}^{\frac{qV}{kT}} - 1\right) \\ &- \frac{n_{\mathrm{i}}qA\left(x_{\mathrm{p}}+x_{\mathrm{n}}\right)}{2\sqrt{\tau_{\mathrm{n0}}\tau_{\mathrm{p0}}}}\left(\mathrm{e}^{\frac{qV}{2kT}} - 1\right) \end{aligned} \tag{11}$$

In Eq. (11), the first two terms on the right side of the equation are photogenerated current I_{ph}. The last two terms are the charge carrier injection current and recombination current, which can be defined as I_{d1} and I_{d2}, respectively. And they are independent of laser irradiance intensity and determined by the forward bias voltage and temperature of the PV cell. Eq. (11) yields the following equation.

$$I_{\mathrm{ph}} = \frac{\eta_0 P\lambda q D_{\mathrm{p}}\alpha^2\tau_{\mathrm{p}}}{hc\left(\alpha^2 L_{\mathrm{p}}^2 - 1\right)}\mathrm{e}^{-\alpha(W_{\mathrm{n}}-x_{\mathrm{n}})} + \frac{\eta_0 P\lambda q D_{\mathrm{n}}\alpha^2\tau_{\mathrm{n}}}{hc\left(\alpha^2 L_{\mathrm{n}}^2 - 1\right)}\mathrm{e}^{-\alpha(W_{\mathrm{n}}+x_{\mathrm{p}})} \tag{12}$$

$$I_{\mathrm{d1}} = \left(\frac{qAD_{\mathrm{p}}n_{\mathrm{i}}^2}{L_{\mathrm{p}}N_{\mathrm{D}}} + \frac{qAD_{\mathrm{n}}n_{\mathrm{i}}^2}{L_{\mathrm{n}}N_A}\right)\left(\mathrm{e}^{\frac{qV}{kT}} - 1\right) = I_{\mathrm{o1}}\left(\mathrm{e}^{\frac{qV}{kT}} - 1\right) \tag{13}$$

$$I_{\mathrm{d2}} = \left(\frac{n_{\mathrm{i}}qA\left(x_{\mathrm{p}}+x_{\mathrm{n}}\right)}{2\sqrt{\tau_{\mathrm{n0}}\tau_{\mathrm{p0}}}}\right)\left(\mathrm{e}^{\frac{qV}{2kT}} - 1\right) = I_{\mathrm{o2}}\left(\mathrm{e}^{\frac{qV}{2kT}} - 1\right) \tag{14}$$

$$I = I_{\mathrm{ph}} - I_{\mathrm{d1}} - I_{\mathrm{d2}} = I_{\mathrm{ph}} - I_{\mathrm{d}} \tag{15}$$

The equivalent circuit model of the PV cell can be obtained from Eqs. (12)-(15), as shown in FIGURE 3(a). When considering the parasitic resistance caused by physical structure, manufacturing process, material properties and leakage current of the PV cell. In order to more accurately express the output characteristics of the PV cell, the ideal equivalent circuit model in FIGURE 3(a) is modified into the double diode model as shown in FIGURE 3(b).

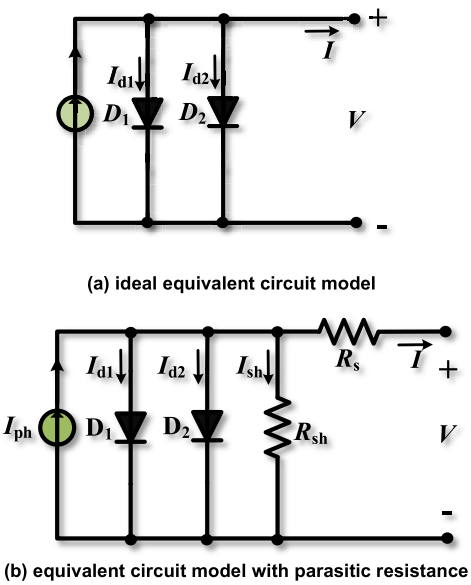

FIGURE 3. Equivalent circuit model of photovoltaic cell.

B. DYNAMIC MATHEMATICAL MODEL AND EQUIVALENT CIRCUIT OF THE PV CELL

The dynamic characteristics of the PV cell include the transient characteristics when laser intensity or equivalent load has a step change and the stability when the laser intensity or load fluctuates with different frequencies and small amplitude. Based on Eqs. (1), (2), this section studies the transient response of output current when laser intensity P changes step and the transient response of dark current when the equivalent load R_0 step changes. Photogenerated current is formed by directional motion of photogenerated carrier. Its lifetime directly determines the dynamic response time of the photogenerated current and the output current according to the expression of photogenerated current (12). Assuming when $t = 0$, the laser intensity received by the PV cell have a step change from 0 W to P, and solve the dynamic continuum equation (1) and (2) to obtain the expression of excess carrier concentration with time t:

$$\begin{aligned}
&\delta n(x,t)\\
&= \frac{\eta_0 P\lambda\alpha \mathrm{e}^{-\alpha(W_\mathrm{n}+x_\mathrm{p})}}{Ahc(\frac{1}{\tau_\mathrm{n}} - D_\mathrm{n}\alpha^2)}\Big[\mathrm{e}^{-\alpha(x-x_\mathrm{p})} - \mathrm{e}^{(D_\mathrm{n}\alpha^2-\frac{1}{\tau_\mathrm{n}})t-\alpha(x-x_\mathrm{p})}\\
&\quad -\frac{1}{\tau_\mathrm{n}}\int_0^t e^{-\frac{\tau}{\tau_\mathrm{n}}}\mathrm{d}\tau\\
&\quad +\frac{2}{\tau_\mathrm{n}\sqrt{\pi}}\int_0^t e^{-\frac{\tau}{\tau_\mathrm{n}}}\mathrm{d}\tau\int_0^{\frac{(x-x_\mathrm{p})\sqrt{\tau_\mathrm{n}}}{2L_\mathrm{n}\sqrt{\tau}}} e^{-\eta^2}\mathrm{d}\eta\alpha^2 D_\mathrm{n} e^{-\frac{t}{\tau_\mathrm{n}}}\int_0^t\\
&\quad \times \mathrm{e}^{\alpha^2 D_\mathrm{n}\tau}\mathrm{d}\tau\\
&\quad -\alpha^2 D_\mathrm{n} e^{-\frac{t}{\tau_\mathrm{n}}}\frac{2}{\sqrt{\pi}}\int_0^t e^{\alpha^2 D_\mathrm{n}\tau}\mathrm{d}\tau\int_0^{\frac{(x-x_\mathrm{p})\sqrt{\tau_\mathrm{n}}}{2L_\mathrm{n}\sqrt{t-\tau}}} e^{-\eta^2}\mathrm{d}\eta\Big]
\end{aligned} \tag{16}$$

$$\begin{aligned}
&\delta p(x,t)\\
&= \frac{\eta_0 P\lambda\alpha \mathrm{e}^{-\alpha(W_\mathrm{n}-x_\mathrm{n})}}{Ahc(\frac{1}{\tau_\mathrm{p}} - D_\mathrm{p}\alpha^2)}\Big[\mathrm{e}^{-\alpha(x+x_\mathrm{n})} - \mathrm{e}^{(D_\mathrm{p}\alpha^2-\frac{1}{\tau_\mathrm{p}})t-\alpha(x+x_\mathrm{n})}\\
&\quad -\frac{1}{\tau_\mathrm{p}}\int_0^t e^{-\frac{\tau}{\tau_\mathrm{p}}}\mathrm{d}\tau\\
&\quad +\frac{2}{\tau_\mathrm{p}\sqrt{\pi}}\int_0^t e^{-\frac{\tau}{\tau_\mathrm{p}}}\mathrm{d}\tau\int_0^{\frac{(x+x_\mathrm{n})\sqrt{\tau_\mathrm{p}}}{2L_\mathrm{p}\sqrt{\tau}}} e^{-\eta^2}\mathrm{d}\eta\\
&\quad +\alpha^2 D_\mathrm{p} e^{-\frac{t}{\tau_\mathrm{p}}}\int_0^t \mathrm{e}^{\alpha^2 D_\mathrm{p}\tau}\mathrm{d}\tau\\
&\quad -\alpha^2 D_\mathrm{p}\mathrm{e}^{-\frac{t}{\tau_\mathrm{p}}}\frac{2}{\sqrt{\pi}}\int_0^t e^{\alpha^2 D_\mathrm{p}\tau}\mathrm{d}\tau\int_0^{\frac{(x+x_\mathrm{n})\sqrt{\tau_\mathrm{p}}}{2L_\mathrm{p}\sqrt{t-\tau}}} e^{-\eta^2}\mathrm{d}\eta\Big]
\end{aligned} \tag{17}$$

The dynamic photogenerated current $i_\mathrm{ph}(t)$ satisfies Eq. (18):

$$\begin{aligned}
i_\mathrm{ph}(t) &= A\times\left[J_\mathrm{p}(-x_\mathrm{n},t) + J_\mathrm{n}(x_\mathrm{p},t)\right]\\
&= -qAD_\mathrm{p}\frac{\partial(\delta p(x,t))}{\partial x}|_{x=-x_\mathrm{n}} + qAD_\mathrm{n}\frac{\partial(\delta n(x,t))}{\partial x}|_{x=x_\mathrm{p}}
\end{aligned} \tag{18}$$

Substituting Eqs. (16) and (17) into Eq. (18), $i_\mathrm{ph}(t)$ can be obtained:

$$\begin{aligned}
i_\mathrm{ph}(t) &= \frac{q\eta_0 P\lambda\alpha^2 L_\mathrm{n}^2 \mathrm{e}^{-\alpha(W_\mathrm{n}+x_\mathrm{p})}}{hc\left(1-L_\mathrm{n}^2\alpha^2\right)}\left\{\frac{1}{\alpha D_\mathrm{n}\sqrt{\tau_\mathrm{n}}}\mathrm{erf}(\frac{\sqrt{t}}{\sqrt{\tau_\mathrm{n}}})\right.\\
&\quad \left. - \mathrm{e}^{(D_\mathrm{n}\alpha^2-\frac{1}{\tau_\mathrm{n}})t}\mathrm{erf}(\frac{\sqrt{t}}{\alpha\sqrt{D_\mathrm{n}}}) - \left[1-\mathrm{e}^{(D_\mathrm{n}\alpha^2-\frac{1}{\tau_\mathrm{n}})t}\right]\right\}\\
&\quad - \frac{q\eta_0 P\lambda\alpha^2 L_\mathrm{p}^2 \mathrm{e}^{-\alpha(W_\mathrm{n}-x_\mathrm{n})}}{hc\left(1-L_\mathrm{p}^2\alpha^2\right)}\left\{\left[1-\mathrm{e}^{(D_\mathrm{p}\alpha^2-\frac{1}{\tau_\mathrm{p}})t}\right]\right.\\
&\quad \left. + \frac{1}{\alpha D_\mathrm{p}\sqrt{\tau_\mathrm{p}}}\mathrm{erf}(\frac{\sqrt{t}}{\sqrt{\tau_\mathrm{p}}}) - \mathrm{e}^{(D_\mathrm{p}\alpha^2-\frac{1}{\tau_\mathrm{p}})t}\mathrm{erf}(\frac{\sqrt{t}}{\alpha\sqrt{D_\mathrm{p}}})\right\}
\end{aligned} \tag{19}$$

Eq. (19) is the transient photogenerated current equation of the PV cell when the laser intensity P step changes.

When the laser intensity and temperature are constant, the step change of the load R_0 will lead to the step change of its forward bias voltage V. According to Eqs (13) and (14), the dark current I_d of the PV cell is a function of forward bias voltage V and temperature T, and it is independent with laser intensity. The equations of the dynamic carrier concentration with time when the forward bias voltage changes from 0 V step to V, can be obtained from Eqs (1) and (2):

$$\begin{aligned}
\delta n(x,t) &= n_{\mathrm{p}0}(\mathrm{e}^{\frac{qV}{kT}}-1)\left\{\mathrm{e}^{-\frac{t}{\tau_\mathrm{n}}}\mathrm{erfc}\left[\frac{(x-x_\mathrm{p})\sqrt{\tau_\mathrm{n}}}{2L_\mathrm{n}\sqrt{t}}\right]\right.\\
&\quad + \frac{1}{\tau_\mathrm{n}}\int_0^t \mathrm{e}^{-\frac{\tau}{\tau_\mathrm{n}}}\mathrm{d}\tau\\
&\quad \left. - \frac{2}{\tau_\mathrm{n}\sqrt{\pi}}\int_0^t \mathrm{e}^{-\frac{\tau}{\tau_\mathrm{n}}}\mathrm{d}\tau\int_0^{\frac{(x-x_\mathrm{p})\sqrt{\tau_\mathrm{n}}}{2L_\mathrm{n}\sqrt{\tau}}} \mathrm{e}^{-u^2}\mathrm{d}u\right\}
\end{aligned} \tag{20}$$

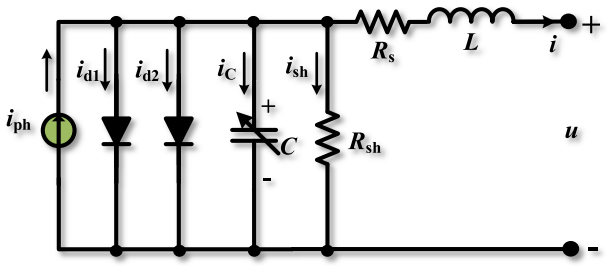

FIGURE 4. Dynamic equivalent circuit model of the PV cell.

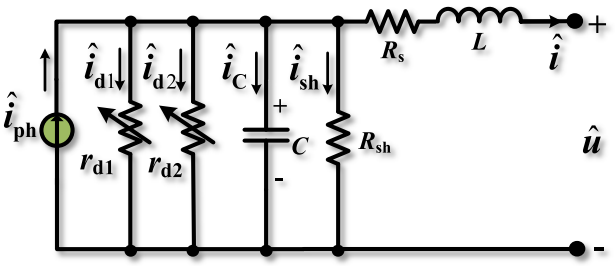

FIGURE 5. Equivalent small signal circuit model of the PV cell.

$$\delta p(x,t) = p_{n0}(e^{\frac{qV}{kT}} - 1)\left\{ e^{-\frac{t}{\tau_p}} \operatorname{erfc}\left[\frac{(x+x_n)\sqrt{\tau_p}}{2L_p\sqrt{t}}\right] + \frac{1}{\tau_p}\int_0^t e^{-\frac{\tau}{\tau_p}} d\tau - \frac{2}{\tau_p\sqrt{\pi}}\int_0^t e^{-\frac{\tau}{\tau_p}} d\tau \int_0^{\frac{(x+x_n)\sqrt{\tau_p}}{2L_p\sqrt{\tau}}} e^{-u^2} du \right\} \quad (21)$$

Substituting Eq. (20) and Eq. (21) into Eq. (8), the dark current can be expressed as

$$i_d(t) = (e^{\frac{qV}{kT}} - 1)\left\{ \frac{AqD_n n_i^2}{L_n N_A}\left[e^{-\frac{t}{\tau_n}} \frac{\sqrt{\tau_n}}{\sqrt{t}\sqrt{\pi}} + \operatorname{erfc}\left(\sqrt{\frac{t}{\tau_n}}\right)\right] + \frac{AqD_p n_i^2}{L_p N_D}\left[e^{-\frac{t}{\tau_p}} \frac{\sqrt{\tau_p}}{\sqrt{t}\sqrt{\pi}} + \operatorname{erfc}\left(\sqrt{\frac{t}{\tau_p}}\right)\right]\right\} + I_d \quad (22)$$

Based on the static circuit model in FIGURE 3(b) and Eq (22), the dynamic model can be established considering the parasitic capacitance C and inductance L, as shown in FIGURE 4.

C. SMALL SIGNAL CIRCUIT MODEL OF THE PV CELL

The photogenerated current I_{ph} can be obtained from the dynamic model of the PV cell in FIGURE 4 when the laser intensity is constant. The transient current $i_c(t)$ of the capacitor C is the transient component of the dark current $i_d(t)$, which can be expressed as $i_d(t)$-I_d. The expressions of dynamic capacitor C and capacitor current i_c can be obtained

$$C(t) = \frac{d(\int i_C(t)dt)}{dV_C} = \frac{\int (i_d(t) - I_d)dt}{dV_C} \quad (23)$$

$$i_c(t) = (e^{\frac{qV}{kT}} - 1)Aqn_i^2\left\{ \frac{D_n}{L_n N_A}\left[e^{-\frac{t}{\tau_n}} \frac{\sqrt{\tau_n}}{\sqrt{t}\sqrt{\pi}} + \operatorname{erfc}\left(\sqrt{\frac{t}{\tau_n}}\right)\right] + \frac{D_p}{L_p N_D}\left[e^{-\frac{t}{\tau_p}} \frac{\sqrt{\tau_p}}{\sqrt{t}\sqrt{\pi}} + \operatorname{erfc}\left(\sqrt{\frac{t}{\tau_p}}\right)\right]\right\} \quad (24)$$

According to the FIGURE 4 and Eq. (24), the dynamic capacitance C is determined by the current I_d at steady-state operating point (I_d, V). Therefore, the equivalent dynamic capacitance $C(V)$ at any operating point can be obtained:

$$C(V) = \lim_{t\to\infty} C(t) = \frac{q}{kT} e^{\frac{qV}{kT}}\left\{ \frac{AqD_n n_i^2 \tau_n}{L_n N_A} + \frac{AqD_p n_i^2 \tau_p}{L_p N_D}\right\} \quad (25)$$

In the PV system, the PV cell are cascaded with the DC/DC converter. DC/DC converter is used for achieving the maximum power tracking and maintaining the output power stability. The equivalent output impedance affects the maximum power point and the stability of the LWPT system. Therefore, the small signal model is established to calculate its output impedance. Based on FIGURE 4, the small signal model is proposed in FIGURE 5, where the diode in the dynamic model can be represented by the dynamic resistors r_{d1} and r_{d2}. And the expressions of r_{d1} and r_{d2} can be obtained, Eq. (26) and Eq. (27). Thus, the equivalent output impedance can be expressed as Eq. (28).

$$r_{d1} = \frac{dV_{d1}}{di_{d1}} = \frac{dV_C}{di_{d1}} = \frac{dV_C}{I_{o1}d(e^{\frac{qV_C}{kT}} - 1)} = \frac{kT}{q(I_{d1} + I_{o1})} \quad (26)$$

$$r_{d2} = \frac{dV_{d2}}{di_{d2}} = \frac{dV_C}{di_{d2}} = \frac{dV_C}{I_{o2}d(e^{\frac{qV_C}{2kT}} - 1)} = \frac{2kT}{q(I_{d2} + I_{o2})} \quad (27)$$

$$Z_o(s) = \frac{du(s)}{d\hat{i}(s)} = \frac{r_{d1}r_{d2}R_{sh} + r_{d1}R_{sh}R_s + r_{d2}R_{sh}R_s + r_{d1}r_{d2}R_s}{b} + \frac{(Cr_{d1}r_{d2}R_sR_{sh} + r_{d1}R_{sh}L + r_{d2}R_{sh}L + r_{d1}r_{d2}L)\,s}{b} + \frac{LCr_{d1}r_{d2}R_{sh}s^2}{b} \quad (28)$$

Here

$$b = r_{d1}R_{sh} + r_{d2}R_{sh} + r_{d1}r_{d2} + sCr_{d1}r_{d2}R_{sh} \quad (29)$$

D. LARGE SIGNAL CIRCUIT MODEL OF THE PV CELL

To evaluate the dynamic output performance of the PV cell when the laser intensity or equivalent load encounters the large disturbance, the equivalent large signal circuit model is established as shown in FIGURE 6. The I-V characteristic curve is linearized with the piecewise linearization method, as shown present FIGURE 7.

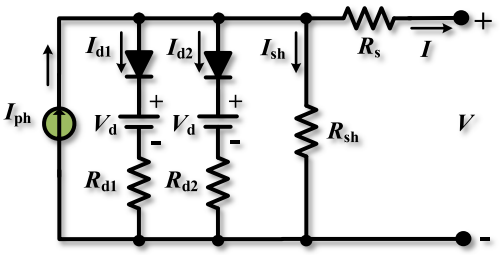

FIGURE 6. Equivalent large signal circuit model of the PV cell.

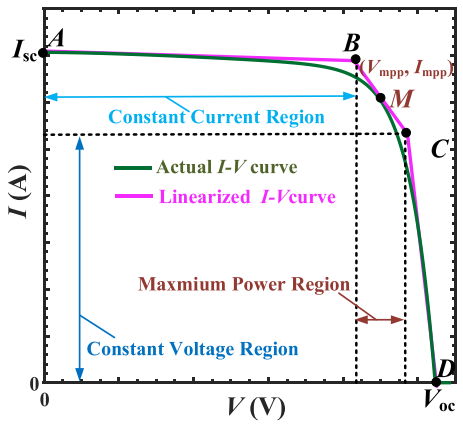

FIGURE 7. The proposed piecewise linearization method of the *I-V* curve.

The piecewise linearization method of the *I-V* curve is as follows:

(a) In the constant current region, the tangent line at the point A (0, I_{sc}) is selected as the linearized curve of the *I-V* characteristic curve. According to FIGURE 6, the following expressions can be obtained:

$$I_{sc} = I_{ph} - \frac{I_{sc}R_s - V_d}{R_d} - \frac{I_{sc}R_s}{R_{sh}} \tag{30}$$

$$R_d = \frac{(I_{sc}R_s - V_d)\,R_{sh}}{(I_{ph} - I_{sc})\,R_{sh} - R_s I_{sc}} \tag{31}$$

In the constant current region, the equivalent linear model can be described by the ideal current source in parallel with the equivalent resistance R_{eq}. The equivalent circuit model of the PV cell can be expressed in FIGURE 8(a). Here R_{eq} is obtained from R_d and R_{sh} in parallel as follows:

$$R_{eq} = \frac{(I_{sc}R_s - V_d)\,R_{sh}}{(I_{ph} - I_{sc})\,R_{sh} - V_d} \tag{32}$$

Based on the equivalent circuit model in the constant current region, the linearized equation (33) of the *I-V* characteristic curve can be obtained:

$$I = -\frac{1}{R_{eq}}V + I_{ph} - \frac{R_s}{R_{eq}} \tag{33}$$

(b) In the maximum power area, *I-V* characteristic curve are described by the tangent line at the maximum power point $M(V_{mpp}, I_{mpp})$. At this point, dP/dV satisfies Eq. (34). The equivalent circuit model can be equivalent to FIGURE 8(b).

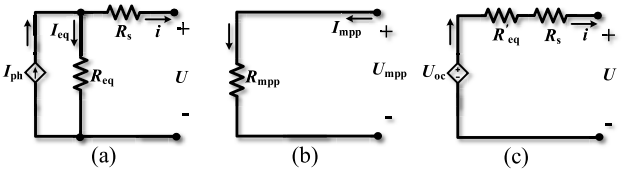

FIGURE 8. Equivalent large signal circuit model of the PV cell, (a) equivalent circuit model in the constant current region; (b) equivalent circuit model in the maximum power region; (c) equivalent circuit model in the constant voltage region.

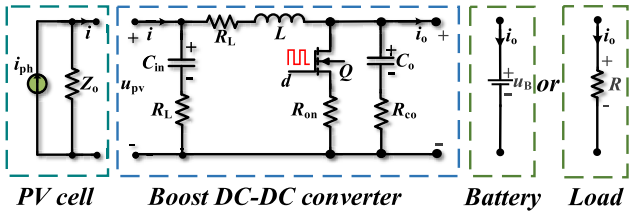

FIGURE 9. Equivalent circuit model of the LWPT system.

The *I-V* characteristic curve equation can be replaced by Eq. (35) at its maximum power point.

$$\left.\frac{\mathrm{d}(VI)}{\mathrm{d}V}\right|_{V=V_{mpp}} = I_{mpp} + V_{mpp}\left.\frac{\mathrm{d}I}{\mathrm{d}V}\right|_{V=V_{mpp}} = I_{mpp} + \frac{V_{mpp}}{R_{mpp}} = 0 \tag{34}$$

$$I = -\frac{I_{mpp}}{V_{mpp}}V + 2I_{mpp} \tag{35}$$

(c) In the constant voltage area, the tangent equation at the point (V_{oc},0) is selected as the linearization curve of the *I-V* characteristic curve. At this point, the equivalent linear model can be equivalent to ideal constant voltage source and equivalent resistance in series. According to FIGURE 6, it can be obtained as follows:

$$I_{ph} = \frac{V_{oc} - V_d}{R_d} + \frac{V_{oc}}{R_{sh}} \tag{36}$$

$$R'_d = \frac{(V_{oc} - V_d)\,R_{sh}}{(I_{ph}R_{sh} - V_{oc})} \tag{37}$$

$$R'_{eq} = \frac{(V_{oc} - V_d)\,R_{sh}}{I_{ph}R_{sh} - V_{oc}} \tag{38}$$

The equivalent circuit model in the constant voltage region is shown in FIGURE 8(c). The linearized equation of *I-V* characteristic curve in this region can be obtained:

$$I = -\frac{1}{R'_{eq} + R_s}V + \frac{1}{R'_{eq} + R_s}V_{oc} \tag{39}$$

E. EQUIVALENT CIRCUIT MODEL OF THE LWPT SYSTEM

To study the effect of the laser intensity or load disturbance on the stability of the LWPT system, the equivalent circuit model based on the boost DC-DC converter is established as shown in FIGURE 9.

According to the equivalent circuit model in FIGURE 9, the equivalent small signal model of LWPT system can be

established based on the state-space averaging method. When the laser intensity is disturbed, the transfer function on the input voltage u_{pv} to photogenerated current i_{ph} of the LWPT system with resistive load R and the constant voltage load (battery) u_B are as follows:

$$G_{\widehat{u}_{pv}\_\widehat{i}_{ph}} = \left.\frac{\widehat{u}_{pv}(s)}{\widehat{i}_{ph}(s)}\right|_{\widehat{d}(s)=0} = \frac{Z_1\left(sL + R_{eq} + \frac{A^2D'^2}{sC+B}\right)}{Z_1 + sL + R_{eq} + \frac{A^2D'^2}{sC+B}} \quad (40)$$

$$G_{\widehat{u}_{pv}\_\widehat{i}_{ph}} = \left.\frac{\widehat{u}_{pv}(s)}{\widehat{i}_{ph}(s)}\right|_{\substack{\widehat{d}(s)=0 \\ \widehat{u}_B(s)=0}} = \frac{sL + R_2}{1 + \frac{sL+R_2}{Z_1}} \quad (41)$$

The MPPT algorithm can control and adjust the output power of the PV cell by controlling the duty cycle d of the control signal PWM driving the DC-DC converter. The transfer function on the input voltage u_{pv} to the control signal d (duty cycle) of the DC-DC converter with resistive load R and the constant voltage load (battery) u_B are as follows:

$$G_{\widehat{u}_{pv}\_\widehat{d}} = \left.\frac{\widehat{u}_{pv}(s)}{\widehat{d}(s)}\right|_{\widehat{i}_{ph}(s)=0} = \frac{A^2D'I_L + (AU_c + R_1I_L)(sC+B)}{sC + B + Z_1(sC+B)(sL+R_{eq})} \quad (42)$$

$$G_{\widehat{u}_{pv}\_\widehat{d}} = \left.\frac{\widehat{u}_{pv}(s)}{\widehat{d}(s)}\right|_{\substack{\widehat{u}_B(s)=0 \\ \widehat{i}_{ph}(s)=0}} = \frac{(R_L + R_{on})I_L + U_B}{1 + \frac{sL+R_2}{Z_1}} \quad (43)$$

where the transfer function Eqs (40) to (43) do not depend on the type of specific MPPT algorithm. The specific derivation process and parameters can be seen in Appendix.

III. NUMERICAL RESULTS AND DISCUSSION

A. THE PARAMETER IDENTIFICATION OF THE STATIC MODEL

From the equivalent circuit model shown in FIGURE 3(b), the transcendental equation can be obtained as follows:

$$I = I_{ph} - I_{o1}\left[\exp\left(\frac{V + IR_s}{V_t}\right) - 1\right] - I_{o2}\left[\exp\left(\frac{V + IR_s}{V_t}\right) - 1\right] - \frac{V + IR_s}{R_{sh}} \quad (44)$$

In Eq (40), R_s and R_{sh} are unknown parameters. To accurately characterize the I-V characteristic using the equivalent circuit equation, it is necessary to extract and identify the unknown parameters in the model. Eq (44) is applied to fit the measured I-V data of the PV cell, and the value of R_s and R_{sh} can be obtained.

According to the physical parameters of gallium arsenide PV cell (in Table 1) and the Eq (44), the static output characteristic curves of the PV cell under different laser intensity are obtained. The lifetime of the carrier is set as100 ns. The model curve is gradually close to the experimental data of output voltage and current under different laser intensity by dynamically adjusting the unknown parameters R_s and R_{sh}. Based on the parameter values in Table 1, the fitting results are shown in the FIGURE 10, where the solid line is the curve of the theoretical model, and the scattered points are the experimental data. In FIGURE 10, it can be found that the established model can well fit the actual output characteristics of the PV cell. Meanwhile, the method and model used in this paper are verified. The over-estimate power at MPP is from the theoretical photo-generated current I_{ph} relative to its actual value. In addition, because the temperature T is a slowly changing variable, it set as a constant value (25 °C) in the theoretical model. Due to it is difficult to maintain the temperature completely constant during the test, the increase of the power may cause the small increment of the temperature inside the PV cell, which will decrease the current I_{ph}. Therefore, the test power at MPP less than the theoretical power obtained according to the model.

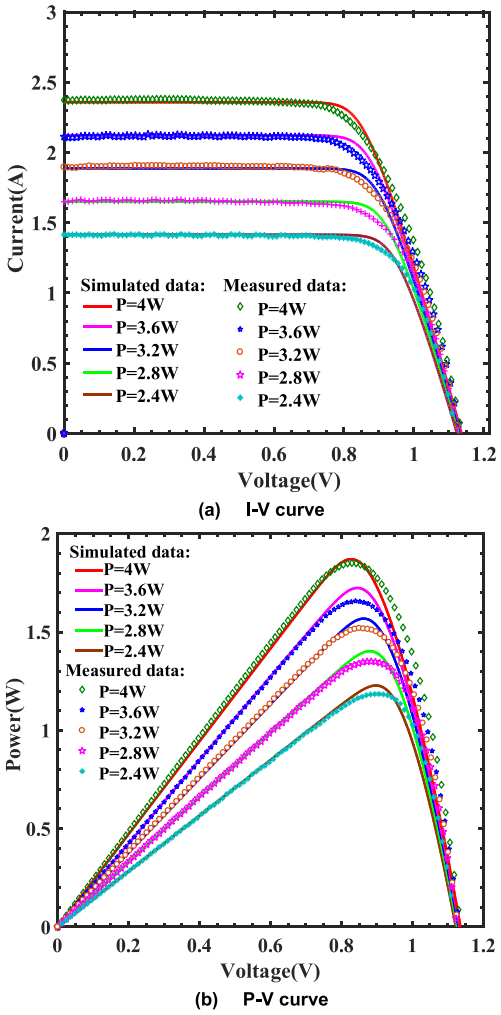

FIGURE 10. The theoretical model curve and experimental data of the PV cell under different laser irradiation.

B. DYNAMIC CHARACTERISTICS OF THE PV CELL UNDER LARGE SIGNAL DISTURBANCE

According to Eq (19) and Table 1, the variation trend of the dynamic current versus time under different carrier lifetimes is presented in FIGURE 11. It can be found that the

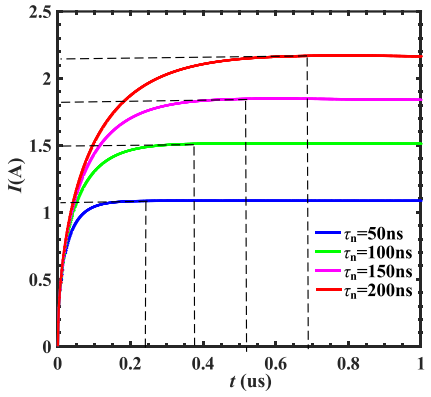

FIGURE 11. Dynamic response of the photo-generated current I_{ph} versus the carrier lifetime when the laser intensity has a step change.

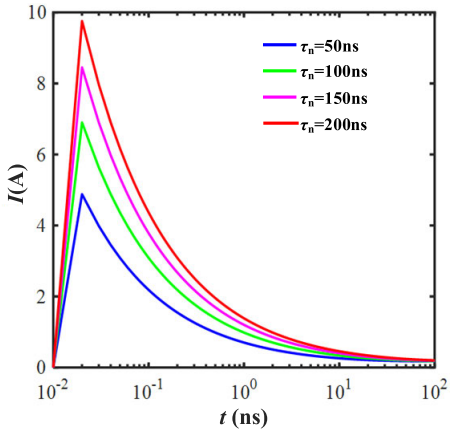

FIGURE 12. Dynamic response of the dark current for the PV cell under different carrier lifetimes when the load has a step change.

photogenerated current presents a step change approximately when the laser intensity P have a step change from 0 W to 3 W, and then tends to be stable. The transient time and steady current increase with the increase of carrier lifetime. The main reason is that the increase of the carrier lifetime means that the decrease of the recombination speed for the carrier. There are more carriers present inside the PV cell at the same time when the laser intensity is constant. Therefore, improving the recombination speed will attenuate the concentration of effective current carrier. Which will decrease the steady-state current I_{ph}, but contribute to improving the dynamic response speed of the photo-generated current.

According to the Eq. (22) of transient dark current $i_d(t)$ when the load R_0 changes abruptly, the dynamic change process of transient dark current with time under different carrier lifetimes can be obtained, as shown in FIGURE 12. The results show that the peak value of the dynamic dark current and the transient time increase with the carrier lifetime. That is because the longer carrier lifetime could contribute to the more carriers existing at the same time, which may significantly increase the peak of the dark current.

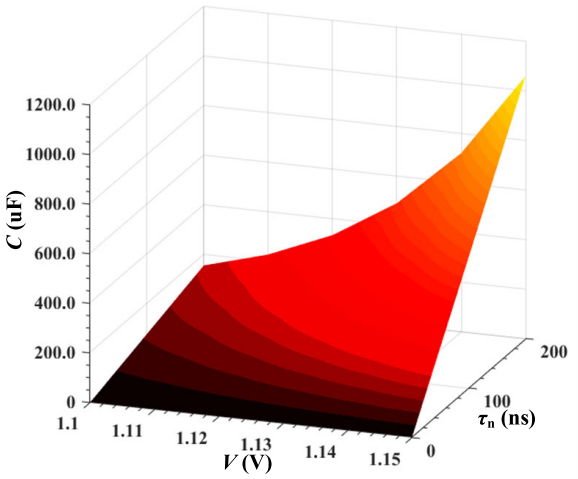

(a) Dynamic capacitance C.

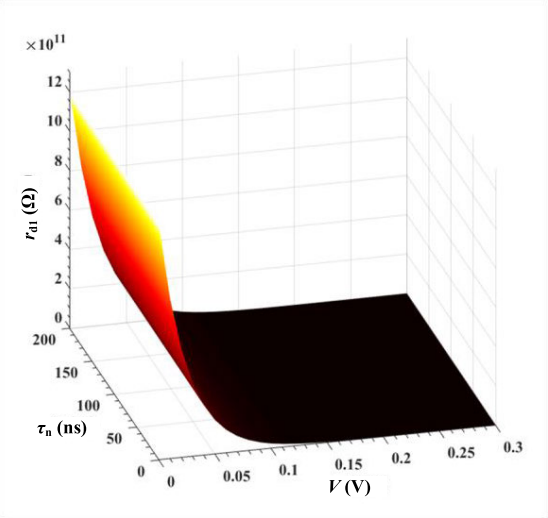

(b) Dynamic resistance r_{d1}.

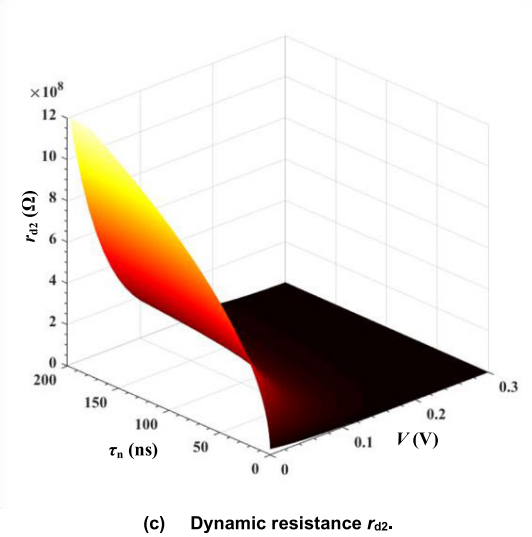

(c) Dynamic resistance r_{d2}.

FIGURE 13. Dynamic parameters in the small signal model of the PV cell.

After the load step change, the forward bias voltage has a transient time and then tends to be stable. Therefore, the dark current has a similar trend with the forward bias voltage,

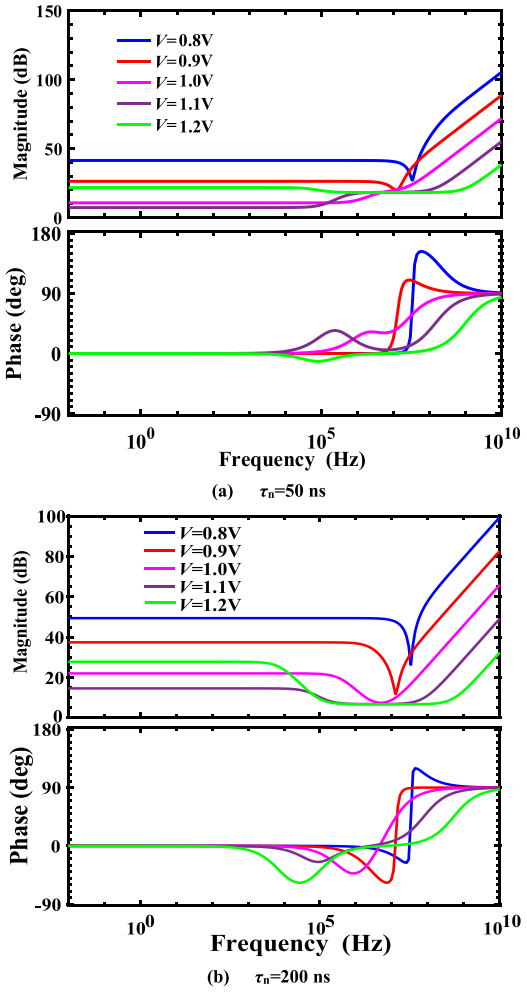

FIGURE 14. Bode diagram of equivalent output impedance of the photovoltaic cell under different forward bias voltage.

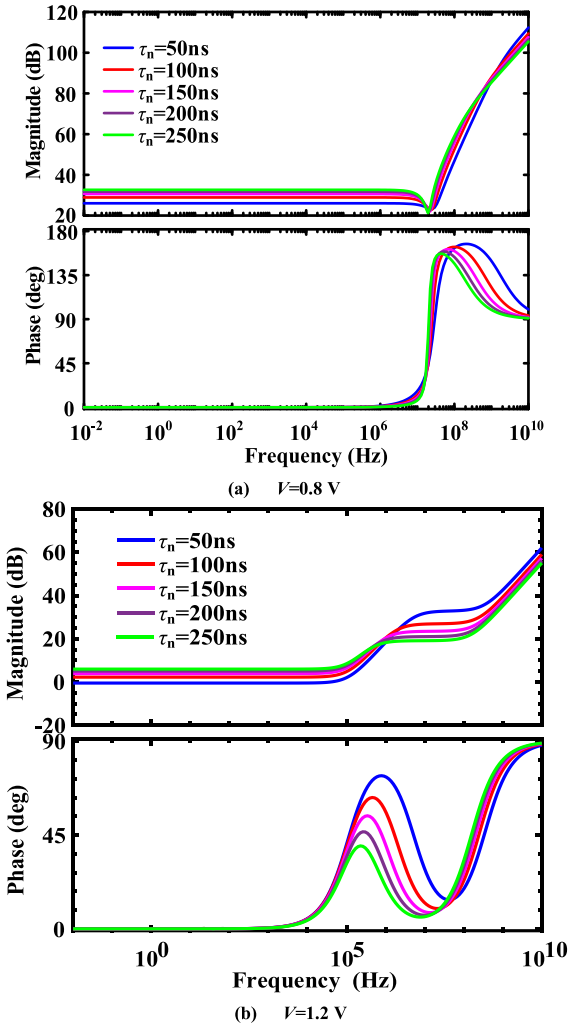

FIGURE 15. Bode diagram of equivalent output impedance of the photovoltaic cell versus carrier lifetimes.

TABLE 2. Parameters and values of the boost DC-DC converter.

Symbol	Value	Symbol	Value
R_L	40 mΩ	C_{in}	47uF
R_{ci}	20 mΩ	C_o	100uF
R_D	37.2 mΩ	L	200uH
R_{on}	10.7mΩ	τ_n	100 ns
R_{co}	20 mΩ	V	0.9 V
U_c	3.3V	P	3 W

which gradually decreases and tends to be stable. According to Eq. (11), when the forward bias voltage is constant, the steady-state dark current I_d is mainly affected by temperature. Therefore, under the same temperature, the steady-state dark currents I_d with different carrier lifetimes remain the same.

C. THE PARAMETER IDENTIFICATION OF THE SMALL SIGNAL MODEL

According to Eqs. (25), (26) and (27), the dynamic model parameters (C, r_{d1} and r_{d2}) of the small signal model can be obtained as a function of forward bias voltage and carrier lifetime, as shown in FIGURE 13(a),(b) and (c). The value of dynamic capacitance C and dynamic resistances (r_{d1} and r_{d2}) have obvious differences at different points of the I-V characteristic curve. It can be found that the dynamic capacitance value and dynamic resistances value increase and decrease respectively with the increase of voltage V. Moreover, in FIGURE 13(a), in the constant current equivalent zone ($V < 0.8$ V in FIGURE 10), the dynamic capacitance value is small and negligible. In the constant voltage equivalent zone ($V > 1.1$ V, in FIGURE 10), the dynamic capacitance value increases with the carrier lifetimes. In FIGURE 13(a) and (b), the dynamic resistance r_{d1} and r_{d2} decrease with the voltage V and increase with the carrier lifetimes. The increase of the dynamic capacitance value with the carrier lifetime can explain why the transition time of the photo-generated current $i_{ph}(t)$ increase with the carrier lifetime when the laser intensity step changes. Meanwhile, the larger dynamic resistance limits the PN junction diode current I_{d1} and I_{d2}.

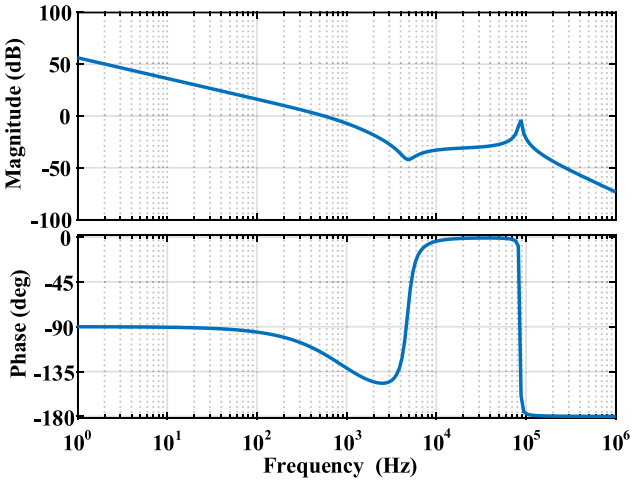

(a) Bode diagram of the transfer function on the input voltage u_{pv} to photogenerated current i_{ph} for the LWPT system with resistive load.

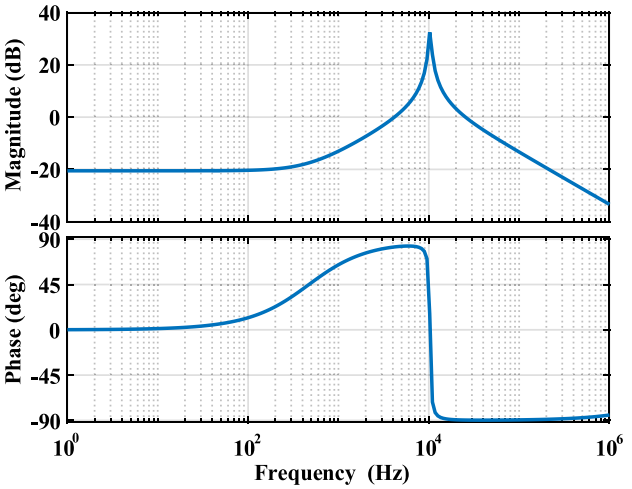

(b) Bode diagram of the transfer function on the input voltage u_{pv} to photogenerated current i_{ph} for the LWPT system with constant voltage load u_B.

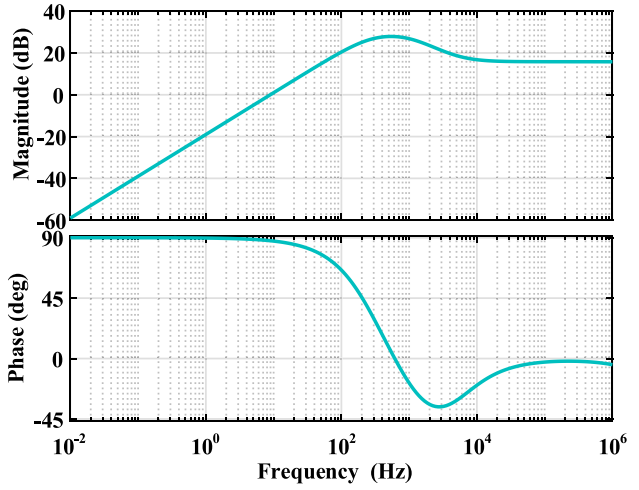

(c) Bode diagram of the transfer function on the input voltage u_{pv} to the control signal d for the LWPT system with resistive load R.

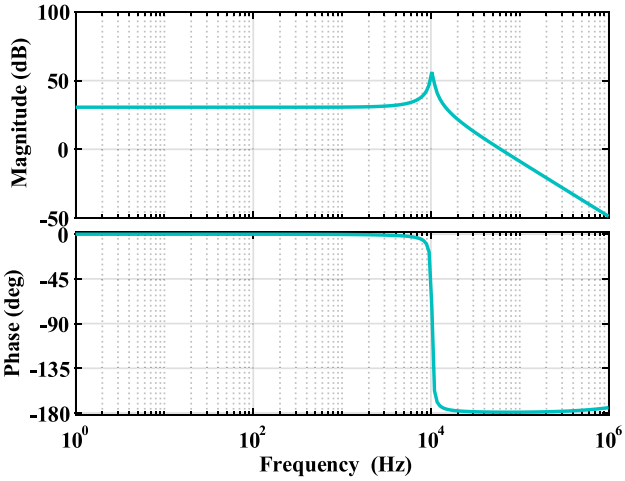

(d) Bode diagram of the transfer function on the input voltage u_{pv} to the control signal d for the LWPT system with constant voltage load u_B.

FIGURE 16. Bode diagram of equivalent output impedance of the photovoltaic cell under different forward bias voltage.

This could illustrate that the steady output current I of the PV cell with longer carrier lifetimes is larger according to Eq. (15).

D. EQUIVALENT OUTPUT IMPEDANCE OF THE PV CELL

As the input power supply of the DC-DC converter, whether the equivalent output impedance of the PV cell matches the equivalent input impedance of the DC-DC converter determines the stability of the LWPT system. To maintain the stability of the LWPT system, the output impedance of the PV cell should be minimized within the operating frequency range than the equivalent input impedance of the DC-DC converter. Based on Eq. (28) and Table 1, the Bode diagram of the output impedance under different carrier lifetimes and load voltages can be obtained, as shown in FIGURE14 and FIGURE 15. The equivalent output impedance is significantly affected by the output voltage V (forward bias voltage) and decreases with it. It means that the equivalent output impedance has significant differences at different operating points. It remains stable at low frequency band and becomes unstable at high frequency band. On the other hand, the equivalent output impedance is negatively correlated with carrier lifetime in the low frequency band. In the high frequency band, the correlation is positive and the equivalent output impedance increase significantly. Even so, at the same static operating point, the carrier lifetime has little influence on its stability. In a word, when the frequency of disturbance signal is low, the LWPT system can maintain open-loop stability, while when the frequency is high, a closed-loop control circuit will be essential to realize the system stability.

E. STABILITY OF THE LWPT SYSTEM

According to the parameter values of the boost DC-DC converter in TABLE 2, the Bode diagram of the transfer function in the Eqs (40) to (43) can be obtained when the system operates at the MPP ($V = V_{mpp}$), as shown in FIGURE 16.

From the Bode diagram in FIGURE 16 (a), the magnitude stability margin increases and phase stability margin decreases with the frequency in the low band (1 Hz to 2kHz). That is because with the increase of frequency, the input filter capacitance can filter the disturbance. However, when the frequency is more than 100 kHz, the phase stability margin will not exist. The main reason is that the parasitic parameters in the circuit are sensitive at high frequency conditions. At this time, the input voltage of the LWPT system with resistive load will be unstable when the laser intensity disturbance causes the photocurrent i_{ph} fluctuation. From the Bode diagram in FIGURE 16 (b), it can be found that the magnitude stability margin decreases and phase stability margin increases with the disturbance frequency at the low frequency band (1 Hz to 10 kHz) in the LWPT system with constant voltage load. But it is the opposite at the high frequency band (10 kHz to 1000 kHz). On the whole, the input voltage of the LWPT system can be stable expect for the frequency band (10 kHz to 20 kHz) with small magnitude stability margin and phase stability margin. From the Bode diagram in FIGURE 16 (c), the magnitude stability margin decreases with the frequency at the frequency band (1 Hz to 100 Hz) and the phase stability margin nearly maintain stable. However, at the high frequency band, the magnitude stability margin keeps essentially constant and the phase stability margin has a noticeable decline then turns to be stable. From the Bode diagram in FIGURE 16 (d), at the frequency band (1 Hz to 10 kHz), the magnitude stability margin and phase stability margin are constant. However, the magnitude stability margin is small may cause the instability of the LWPT system. At the frequency band (10 kHz to 1000 kHz), the phase stability margin approach zero. The system with the open loop control cannot be stable under the disturbance of the duty cycle d.

IV. CONCLUSION

In this paper, the dynamic output characteristics and stability of the PV cell under the laser intensity or load disturbance are studied in LWPT system. The static and dynamic output characteristics equations of the PV cell are creatively derived. The equivalent small signal model and linearized large signal model are established. Moreover, the stability of the LWPT system is analyzed based on the proposed model.

The results of these studies indicate that the explicit *I-V* characteristic equation proposed in this paper can fit well with the measured data and the physical significance of the model parameters are more specific compared with the conventional equivalent circuit model expressed by the implicit transcendental equation. In addition, the output impedance of the PV cell increases with the disturbance frequency of the load and laser intensity. The dynamic response time and the steady-state current of the photocurrent increases with the carrier lifetime. And the model can be effectively used to analyze the stability of the LWPT system.

In conclusion, the models and methods can be effectively used to conduct theoretical analysis and simulation about the stability and dynamic characteristic of the LWPT system.

APPENDIX

The state-space equation of the boost DC-DC converter with the resistive load R as follows:

$$L\frac{d\widehat{i}_L}{dt} = \widehat{u}_{pv} - \left(R_L + R_{on}D + R_D D' + \frac{RR_c}{R+R_c}D'\right)\widehat{i}_L - \frac{RD'}{R+R_c}\widehat{u}_c - \left(R_{on} - R_D - \frac{RR_c}{R+R_c}\right)I_L\widehat{d} + \frac{R}{R+R_c}U_c\widehat{d} \tag{A-1}$$

$$C_o\frac{d\widehat{u}_c}{dt} = \frac{RD'}{R+R_c}\widehat{i}_L - \frac{RI_L}{R+R_c}\widehat{d} - \frac{1}{R+R_c}\widehat{u}_c \tag{A-2}$$

$$\widehat{u}_o = \frac{RR_cD'}{R+R_c}\widehat{i}_L + \frac{R}{R+R_c}\widehat{u}_c - \frac{RR_cI_L}{R+R_c}\widehat{d} \tag{A-3}$$

$$\widehat{i}_{ph} = \widehat{i}_L + \frac{\widehat{u}_{pv}}{\frac{1}{C_i s} + R_{ci}} + \frac{\widehat{u}_{pv}}{Z_o} \tag{A-4}$$

The equations (A-1) to (A-4) can be simplified as follows:

$$sL\widehat{i}_L = \widehat{u}_{pv} - R_{eq}\widehat{i}_L - AD'\widehat{u}_c - R_1I_L\widehat{d} + AU_c\widehat{d} \tag{A-5}$$

$$sC\widehat{u}_c = AD'\widehat{i}_L - AI_L\widehat{d} - B\widehat{u}_c \tag{A-6}$$

$$\widehat{u}_o = ED'\widehat{i}_L + A\widehat{u}_c - EI_L\widehat{d} \tag{A-7}$$

$$\widehat{i}_{ph} = \widehat{i}_L + \frac{\widehat{u}_{pv}}{Z} + \frac{\widehat{u}_{pv}}{Z_o} \tag{A-8}$$

The coefficients in the equations are expressed as follows:

$$R_{eq} = R_L + R_{on}D + R_D D' + \frac{RR_c}{R+R_c}D' \tag{A-9}$$

$$R_1 = R_{on} - R_D - \frac{RR_c}{R+R_c} \tag{A-10}$$

$$A = \frac{R}{R+R_c} \tag{A-11}$$

$$B = \frac{1}{R+R_c} \tag{A-12}$$

$$E = \frac{RR_c}{R+R_c} \tag{A-13}$$

$$Z = \frac{1}{C_i s} + R_{ci} \tag{A-14}$$

$$Z_1 = \frac{ZZ_o}{Z+Z_o} \tag{A-15}$$

The transfer function Eqs (40) and (41) can be obtained:

$$G_{\widehat{u}_{pv}\_\widehat{i}_{ph}} = \left.\frac{\widehat{u}_{pv}(s)}{\widehat{i}_{ph}(s)}\right|_{\widehat{d}(s)=0} = \frac{Z_1\left(sL + R_{eq} + \frac{A^2D'^2}{sC+B}\right)}{Z_1 + sL + R_{eq} + \frac{A^2D'^2}{sC+B}} \tag{40}$$

$$G_{\widehat{u}_{\mathrm{pv}}\_\widehat{i}_{\mathrm{ph}}} = \left.\frac{\widehat{u}_{\mathrm{pv}}(s)}{\widehat{i}_{\mathrm{ph}}(s)}\right|_{\substack{\widehat{d}(s)=0 \\ \widehat{u}_{\mathrm{B}}(s)=0}} = \frac{sL+R_2}{1+\frac{sL+R_2}{Z_1}} \tag{41}$$

The state-space equation of the boost DC-DC converter with the constant voltage load u_{B} are as follows:

$$L\frac{d\widehat{i}_{\mathrm{L}}}{dt} = \widehat{u}_{\mathrm{pv}} - [(R_{\mathrm{L}}+R_{\mathrm{on}})D + (R_{\mathrm{L}}+R_{\mathrm{D}})]\widehat{i}_{\mathrm{L}} - [(R_{\mathrm{L}}+R_{\mathrm{on}})I_{\mathrm{L}} - U_{\mathrm{B}}]\widehat{d} - D'\widehat{u}_{\mathrm{B}} \tag{A-16}$$

$$C_{\mathrm{o}}\frac{d\widehat{u}_{\mathrm{c}}}{dt} = \frac{\widehat{u}_{\mathrm{B}}-\widehat{u}_{\mathrm{c}}}{R_{\mathrm{c}}} \tag{A-17}$$

$$\widehat{u}_{\mathrm{o}} = \widehat{u}_{\mathrm{B}} \tag{A-18}$$

$$\widehat{i}_{\mathrm{ph}} = \widehat{i}_{\mathrm{L}} + \frac{\widehat{u}_{\mathrm{pv}}}{\frac{1}{C_{\mathrm{i}}s}+R_{\mathrm{ci}}} + \frac{\widehat{u}_{\mathrm{pv}}}{Z_{\mathrm{o}}} \tag{A-19}$$

The equations (A-1) to (A-4) can be simplified as follows:

$$sL\widehat{i}_{\mathrm{L}} = \widehat{u}_{\mathrm{pv}} - R2\widehat{i}_{\mathrm{L}} - [(R_{\mathrm{L}}+R_{\mathrm{on}})I_{\mathrm{L}} - U_{\mathrm{B}}]\widehat{d} - D'\widehat{u}_{\mathrm{B}} \tag{A-20}$$

$$sR_{\mathrm{c}}C_{\mathrm{o}}\widehat{u}_{\mathrm{c}} = \widehat{u}_{\mathrm{B}} - \widehat{u}_{\mathrm{c}} \tag{A-21}$$

$$\widehat{u}_{\mathrm{o}} = \widehat{u}_{\mathrm{B}} \tag{A-22}$$

$$\widehat{i}_{\mathrm{ph}} = \widehat{i}_{\mathrm{L}} + \frac{\widehat{u}_{\mathrm{pv}}}{Z} + \frac{\widehat{u}_{\mathrm{pv}}}{Z_{\mathrm{o}}} \tag{A-23}$$

$$R_2 = (R_{\mathrm{L}}+R_{\mathrm{on}})D + R_{\mathrm{L}} + R_{\mathrm{D}} \tag{A-24}$$

The transfer function Eqs (42) and (43) can be obtained:

$$G_{\widehat{u}_{\mathrm{pv}}\_\widehat{d}} = \left.\frac{\widehat{u}_{\mathrm{pv}}(\mathrm{s})}{\widehat{d}(\mathrm{s})}\right|_{\widehat{i}_{\mathrm{ph}}(\mathrm{s})=0} = \frac{A^2D'I_{\mathrm{L}} + (AU_{\mathrm{c}}+R_1I_{\mathrm{L}})(\mathrm{s}C+B)}{\mathrm{s}C+B+Z_1(\mathrm{s}C+B)\left(\mathrm{s}L+R_{\mathrm{eq}}\right)} \tag{42}$$

$$G_{\widehat{u}_{\mathrm{pv}}\_\widehat{d}} = \left.\frac{\widehat{u}_{\mathrm{pv}}(s)}{\widehat{d}(s)}\right|_{\substack{\widehat{u}_{\mathrm{B}}(s)=0 \\ \widehat{i}_{\mathrm{ph}}(s)=0}} = \frac{(R_{\mathrm{L}}+R_{\mathrm{on}})I_{\mathrm{L}}+U_{\mathrm{B}}}{1+\frac{sL+R_2}{Z_1}} \tag{43}$$

REFERENCES

[1] P. E. Glaser, "Power from the sun: Its future," *Science*, vol. 162, no. 3856, pp. 857–861, Nov. 1968, doi: 10.1126/science.162.3856.857.

[2] C. A. Schäfer and D. Gray, "Transmission media appropriate laser-microwave solar power satellite system," *Acta Astronautica*, vol. 79, pp. 140–156, Oct. 2012, doi: 10.1016/j.actaastro.2012.04.010.

[3] K. Jin and W. Zhou, "Wireless laser power transmission: A review of recent progress," *IEEE Trans. Power Electron.*, vol. 34, no. 4, pp. 3842–3859, Apr. 2019, doi: 10.1109/TPEL.2018.2853156.

[4] T.-H. Wu, W.-C. Liu, C.-S. Moo, H.-L. Cheng, and Y.-N. Chang, "An electric circuit model of photovoltaic panel with power electronic converter," in *Proc. IEEE 17th Workshop Control Model. Power Electron. (COMPEL)*, Jun. 2016, pp. 1–6, doi: 10.1109/COMPEL.2016.7556672.

[5] P. Sprangle, B. Hafizi, A. Ting, and R. Fischer, "High-power lasers for directed-energy applications," *Appl. Opt.*, vol. 54, no. 31, pp. F201–F209, Nov. 2015, doi: 10.1364/AO.54.00F201.

[6] W. Nelson, P. Sprangle, and C. C. Davis, "Atmospheric propagation and combining of high-power lasers," *Appl. Opt.*, vol. 55, no. 7, pp. 1757–1764, Mar. 2016, doi: 10.1364/AO.55.001757.

[7] M. Bonnet-Eymard, M. Boccard, G. Bugnon, F. Sculati-Meillaud, M. Despeisse, and C. Ballif, "Optimized short-circuit current mismatch in multi-junction solar cells," *Sol. Energy Mater. Sol. Cells*, vol. 117, pp. 120–125, Oct. 2013, doi: 10.1016/j.solmat.2013.05.046.

[8] L. Peng, Y. Sun, Z. Meng, Y. Wang, and Y. Xu, "A new method for determining the characteristics of solar cells," *J. Power Sources*, vol. 227, pp. 131–136, Apr. 2013, doi: 10.1016/j.jpowsour.2012.07.061.

[9] D. Revati and E. Natarajan, "I-V and P-V characteristics analysis of a photovoltaic module by different methods using MATLAB software," *Mater. Today, Proc.*, vol. 33, pp. 261–269, Jan. 2020, doi: 10.1016/j.matpr.2020.04.043.

[10] S. K. Vankadara, S. Chatterjee, and P. K. Balachandran, "An accurate analytical modeling of solar photovoltaic system considering R_s and R_{sh} under partial shaded condition," *Int. J. Syst. Assur. Eng. Manag.*, vol. 13, pp. 2472–2481, Apr. 2022, doi: 10.1007/s13198-022-01658-6.

[11] G. Ciulla, V. L. Brano, V. D. Dio, and G. Cipriani, "A comparison of different one-diode models for the representation of I-V characteristic of a PV cell," *Renew. Sustain. Energy Rev.*, vol. 32, pp. 684–696, 2014, doi: 10.1016/j.rser.2014.01.027.

[12] K. Tifidat, N. Maouhoub, A. Benahmida, and F. E. A. Salah, "An accurate approach for modeling I-V characteristics of photovoltaic generators based on the two-diode model," *Energy Convers. Manag., X*, vol. 14, May 2022, Art. no. 100205, doi: 10.1016/j.ecmx.2022.100205.

[13] C. Kumar and D. M. Mary, "A novel chaotic-driven Tuna Swarm Optimizer with Newton-Raphson method for parameter identification of three-diode equivalent circuit model of solar photovoltaic cells/modules," *Optik*, vol. 264, Aug. 2022, Art. no. 169379, doi: 10.1016/j.ijleo.2022.169379.

[14] A. R. Jordehi, "Parameter estimation of solar photovoltaic (PV) cells: A review," *Renew. Sustain. Energy Rev.*, vol. 61, pp. 354–371, Aug. 2016, doi: 10.1016/j.rser.2016.03.049.

[15] A. Ortiz-Conde, F. J. García-Sánchez, J. Muci, and A. Sucre-González, "A review of diode and solar cell equivalent circuit model lumped parameter extraction procedures," *Facta Univ. Ser., Elect. Energ.*, vol. 27, no. 1, pp. 57–102, Mar. 2014, doi: 10.2298/FUEE1401057O.

[16] A. Al-Subhi, "Parameters estimation of photovoltaic cells using simple and efficient mathematical models," *Solar Energy*, vol. 209, pp. 245–257, Oct. 2020, doi: 10.1016/j.solener.2020.08.079.

[17] M. Ćalasan, S. H. E. A. Aleem, and A. F. Zobaa, "A new approach for parameters estimation of double and triple diode models of photovoltaic cells based on iterative Lambert W function," *Solar Energy*, vol. 218, pp. 392–412, Apr. 2021, doi: 10.1016/j.solener.2021.02.038.

[18] M. Tripathy, M. Kumar, and P. K. Sadhu, "Photovoltaic system using Lambert W function-based technique," *Solar Energy*, vol. 158, pp. 432–439, Dec. 2017, doi: 10.1016/j.solener.2017.10.007.

[19] K. Ujiie, T. Izumi, T. Yokoyama, and T. Haneyoshi, "Study on dynamic and static characteristics of photovoltaic cell," in *Proc. Power Convers. Conf.-Osaka*, 2002, pp. 810–815, doi: 10.1109/PCC.2002.997624.

[20] D. T. Cotfas, P. A. Cotfas, and S. Kaplanis, "Methods to determine the DC parameters of solar cells: A critical review," *Renew. Sustain. Energy Rev.*, vol. 28, pp. 588–596, Dec. 2013, doi: 10.1016/j.rser.2013.08.017.

[21] L. Qin, S. Xie, C. Yang, and J. Cao, "Dynamic model and dynamic characteristics of solar cell," in *Proc. IEEE ECCE Asia Downunder*, Jun. 2013, pp. 659–663, doi: 10.1109/ECCE-Asia.2013.6579170.

[22] S. Wang, Y. Yu, and W. Hu, "Static and dynamic solar photovoltaic models' parameters estimation using hybrid Rao optimization algorithm," *J. Cleaner Prod.*, vol. 315, Sep. 2021, Art. no. 128080, doi: 10.1016/j.jclepro.2021.128080.

[23] K. A. Kim, C. Xu, L. Jin, and P. T. Krein, "A dynamic photovoltaic model incorporating capacitive and reverse-bias characteristics," *IEEE J. Photovolt.*, vol. 3, no. 4, pp. 1334–1341, Oct. 2013, doi: 10.1109/JPHOTOV.2013.2276483.

[24] S. S. Li. *Semiconductor Physical Electronics*. New York, NY, USA: Springer, 2006, pp. 381–457, doi: 10.1007/0-387-37766-2_12.

[25] D. A. Neamen, *Semiconductor Physics and Devices: Basic Principles*. New York, NY, USA: McGraw-Hill, 2012, pp. 113–171.

ZHENYANG XIONG received the M.S. degree in mechanical engineering from Beihang University, Beijing, China, in 2020. He is currently pursuing the Ph.D. degree with the Aerospace Information Research Institute, Chinese Academy of Sciences, Beijing. His current research interests include power electronics, modeling, control, and laser wireless power transmission technology.

RONG CAI received the B.S. degree from Tsinghua University, China, in 1986, and the M.S. degree from Tongji University, China, in 1989. He is currently a Professor with the Aerospace Information Research Institute, Chinese Academy of Sciences, Beijing, China. His current research interests include system design and simulation of aerostat and research on overall technology of laser wireless energy transmission.

XING DU received the M.S. degree from the Beijing Institute of Technology, China, in 2019. He is currently pursuing the Ph.D. degree with the Aerospace Information Research Institute, Chinese Academy of Sciences, Beijing, China. His current research interest includes underwater laser communication technology.

HAO DU received the B.Sc. degree in electronic information engineering from Beihang University, in 2008, the M.Sc. degree from the University of Nottingham, and the Ph.D. degree from the University of Warwick. The Ph.D. topic is optical wireless communication. He is currently with the Chinese Academy of Sciences, where he is focusing on the topic of optical wireless communication and laser power transmission analysis.

GUONING XU (Senior Member, IEEE) received the Ph.D. degree from Beihang University, Beijing, in 2012. He is currently a Professor with the Aerospace Information Research Institute, Chinese Academy of Sciences, and a Doctoral Supervisor with the University of the Chinese Academy of Sciences, Beijing. Since 2007, he has been involved in advanced power supply, advanced power conversion theory and application, and LTA control theory and applications in near-space extreme environments, for 15 years.